A&A 409, 941–951 (2003)
DOI: 10.1051/0004-6361:20031102

Astronomy & Astrophysics

Star forming cores in L 1251: Maps and molecular abundances

S. Nikolić[1,2], L. E. B. Johansson[1], and J. Harju[3]

[1] Onsala Space Observatory, 439 92 Onsala, Sweden
[2] Astronomical Observatory, Volgina 7, 11160 Belgrade 74, Serbia, Serbia and Montenegro
[3] Helsinki University Observatory, Tähtitorninmäki, PO Box 14, SF-00014 University of Helsinki, Finland

Received 29 April 2003 / Accepted 17 July 2003

Abstract. We have mapped the dense parts of the cometary–shaped, star–forming dark cloud L 1251 in the rotational lines of HCN, HNC, HCO^+ and CS at 3 mm, and observed selected positions in SO, CH_3CCH and rare isotopomers of the mapped molecules. Using the CS line we detected 15 cores with sizes of ~0.1–0.3 pc. New estimates of the fraction of dense gas in the cores yield a revised average SFE of ~10%. Although 3 times lower than the previous estimate, this high SFE still points to externally triggered star formation in the cloud. Around IRAS 22343+7501, the source proposed to drive a previously detected extended CO outflow, our data suggest the existence of either a rotating HCO^+ disk or a dense outflow with a dynamical age of $\sim 2 \times 10^4$ years. A stability check seems to rule out the disk interpretation. We suggest that both continuum sources of Beltrán et al. are protostars each driving its own outflow.
Using methyl acetylene as a thermometer we find indications that at lower temperatures the *A* and *E* species are defined by different partition functions. A "temperature gradient" was found in the cloud, with the highest temperature detected in the head region. The column density ratios derived from these observations and the previously published NH_3 data show in general little variations, but for two exceptional locations. One of these is in the tip of the "head" with high relative SO and NH_3 abundances, and the other is in the "tail" with low CO and HCO^+ column densities with respect to HNC, HCN and NH_3. In the first case the abundance ratios can probably be explained by an advanced stage of chemical evolution assisted by an elevated temperature. The second location is likely to be an example of CO and HCO^+ depletion, and the implication is that also HNC and HCN belong to the molecules which are more resistant against freezing–out than CO and HCO^+.

Key words. ISM: abundances – ISM: clouds – ISM: molecules – ISM: individual objects: L 1251

1. Introduction

The overall star forming efficiency (SFE, defined as the ratio $M_{\rm star}/(M_{\rm star}+M_{\rm gas})$, where $M_{\rm gas}$ is the total gas mass of a molecular cloud and $M_{\rm star}$ is the mass of embedded protostars) for the Galaxy is estimated to be only ~2% (Myers et al. 1986). Similar low SFEs are typical for dark clouds where low – mass stars are born. However, there are clouds with much higher – than – average SFE which indicates that triggered star formation is significant in such cases. For example supernova shock fronts may stimulate the formation of stars through their local effects on density, kinetic temperatures, turbulence, ionization degrees and, as a result, chemical processes.

L 1251 (Lynds 1962) is an example of a dark cloud with an estimated SFE as high as 30% (Kun & Prusti 1993; KP). Both location and cloud morphology suggest that external triggering has contributed to the on – going star formation. This cometary – shaped cloud, at a distance of 300 pc (KP), lies on the Eastern boundary of the Cepheus cloud complex, with the "head" turned towards the center of the Cep – Cas Void (Grenier et al. 1989). At least two supernovas have exploded in this area within the last $\sim 10^6$ years, as indicated by the presence of the major radio – continuum loop, Loop III (Berkhuijsen 1971) and a runaway star HD203854, whose space velocity suggests that it might have been a companion of a supernova some 5×10^5–10^6 years ago (Kun et al. 2000). The Cep – Cas Void is suggested to be created by a third SN (Grenier et al. 1989). However, the estimated age of 10^4 yr means that this SN is much too young to have affected the star forming processes observed now.

Detected Hα stars in the vicinity of the cloud (Kun 1982) and seven embedded YSO (KP) indicate that the cloud is an active low – mass star formation site. Of the YSOs, IRAS 22376+7455 and IRAS 22343+7501, classified as Class I YSOs (Mardones et al. 1997) apparently power two detected CO outflows (Schwartz et al. 1988; Sato & Fukui 1989; Sato et al. 1994). Herbig–Haro objects (Balázs et al. 1992; Eiroa et al. 1995) and H_2O masers (Tóth & Walmsley 1994; Wilking et al. 1994; Xiang & Turner 1995; Claussen et al. 1996; Tóth & Kun 1997) are observed in their vicinity.

The overall distribution of molecular gas in L 1251 has been previously studied by Sato et al. (1994) and

Send offprint requests to: S. Nikolic,
e-mail: silvana@oso.chalmers.se

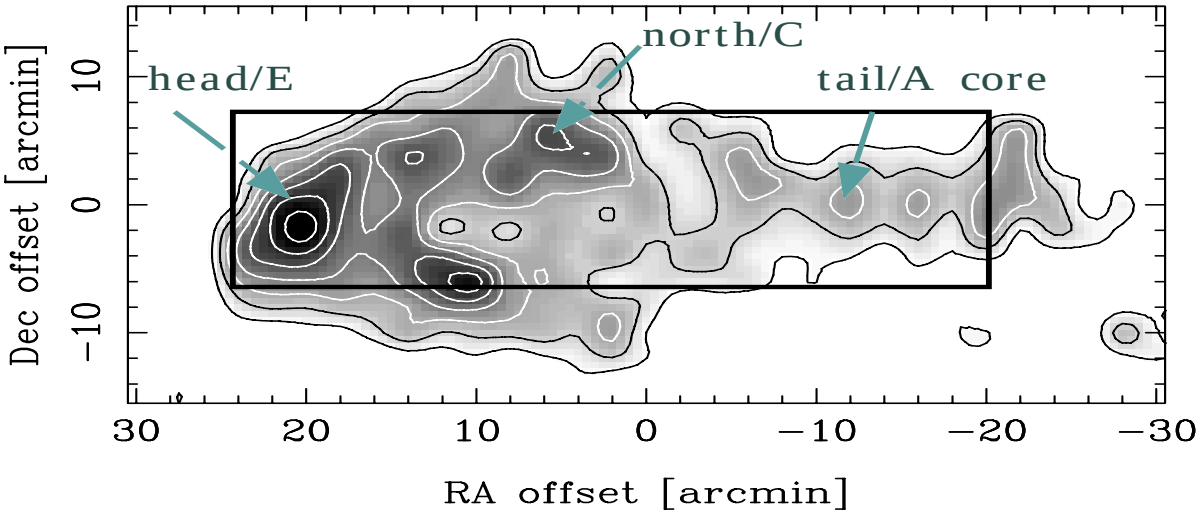

Fig. 1. The ^{13}CO integrated intensity map of L 1251 in the (–2, –6.5) km s^{-1} velocity range obtained by Sato et al. (1994). The center position is RA = $22^{h}33^{m}$ Dec = 74°58′ (1950.0). For the designations of the regions indicated, see the Introduction. The bold–line polygon outlines the area presented in Figs. 2 – 4.

Tóth & Walmsley (1996; TW). Sato et al. identified five C^{18}O cores which they designated as "A" to "E" in increasing RA direction (see Fig. 1). In their ammonia survey, TW discovered three regions of dense gas, "head", "north" and "tail"; the "head" region containing 3 ammonia cores (H 1 to H 3) and the "tail" region consisting of 4 cores (T 1 to T 4), whereas in the "north" a single ammonia core was detected (N, see their Fig. 3). The ammonia "head" group of cores corresponds to core "E" of Sato el al., group "north" to core "C" and the "tail" group to core "A".

Apart from NH_3, commonly used tracers of dense material are CS, HCO^+, and the isomeric molecules HCN and HNC, because their rotational transitions near 3 mm are easy to observe and have critical densities higher that 10^5 cm^{-3}. In this paper we present maps of these molecules in the densest parts of L 1251, and estimate their column densities along with some other molecular species in selected positions. The cloud contains both protostellar and prestellar condensations and shows clear signs of external influence. The physical conditions are therefore likely to vary across the cloud. The aim of this study was to investigate whether any indications of such variations can be traced in the observed molecular lines, and how these possible changes are reflected in chemical abundances.

2. Observations

We used the Onsala Space Observatory's (OSO) 20–m telescope over five observing sessions in 1998, 1999 and 2000 to map the cloud in the HCN (1–0), HNC (1–0), CS (2–1) and HCO^+ (1–0) transitions. Selected positions were subsequently observed in ^{13}CO (1–0), C^{18}O (1–0), H^{13}CN (1–0), HN^{13}C (1–0), C^{34}S (2–1), H^{13}CO$^+$ (1–0), SO ($2_1 - 1_1$) and CH_3CCH ($5_K - 4_K$). The receiver was a SIS mixer with a typical $T_{\rm rec}$ = 100 K (SSB) in the frequency range used. We used a 1600–channel correlator with 20 MHz bandwidth (i.e. a velocity resolution of 0.04 km s^{-1} at 90 GHz). The HPBW of the telescope at 90 GHz is 45″ and the main beam efficiency is 0.6. The pointing was checked by observing several SiO maser sources and we estimate the pointing uncertainty to be about 3″ rms in Az and El. The observations were made either in the frequency (main isotopes) or the dual beam switching mode (rarer isotopes). The chopper–wheel method was used for the calibration, and the intensity scale is given in terms of $T_{\rm A}^*$. We used mostly a grid point spacing of 30″, however, occasionally a 60″ step was used. The data were reduced using the XS[1] package.

3. The maps

Our HCN and HNC (1–0) integrated intensity maps are shown in Fig. 2, and the corresponding CS (2–1) and HCO^+ (1–0) maps are shown in Figs. 3 and 4, respectively. The area mapped in HNC and HCN covers the two ammonia cores in the "head" designated as "H1" and "H2" by TW, the northern part of L 1251, and the cores "T1", "T2" and "T3" in the tail. All these ammonia cores are associated with newly born stars or protostars. The maps in CS and HCO^+ include also the starless core "H3" on the western side of the head core group. Also indicated in these figures are the locations of YSOs and T Tau stars probably associated with the cloud. Labeling of these sources in the upper panel of Fig. 2 follows that of Table 3 of KP.

A comparison between our maps and the NH_3 map of TW reveals two major differences: i) in NH_3 the head and tail regions have similar integrated intensities whereas in HCN, HNC, CS and HCO^+ the head region is clearly brighter. For the latter molecules the higher integrated intensities in the head are due to a larger number of velocity components in the line of sight (see Sect. 3.2); ii) the core around IRAS 22343+7501 (N1a) is not visible in NH_3. Ammonia peaks further up in the north near the T Tau star #9.

[1] The program is developed by P. Bergman, OSO.

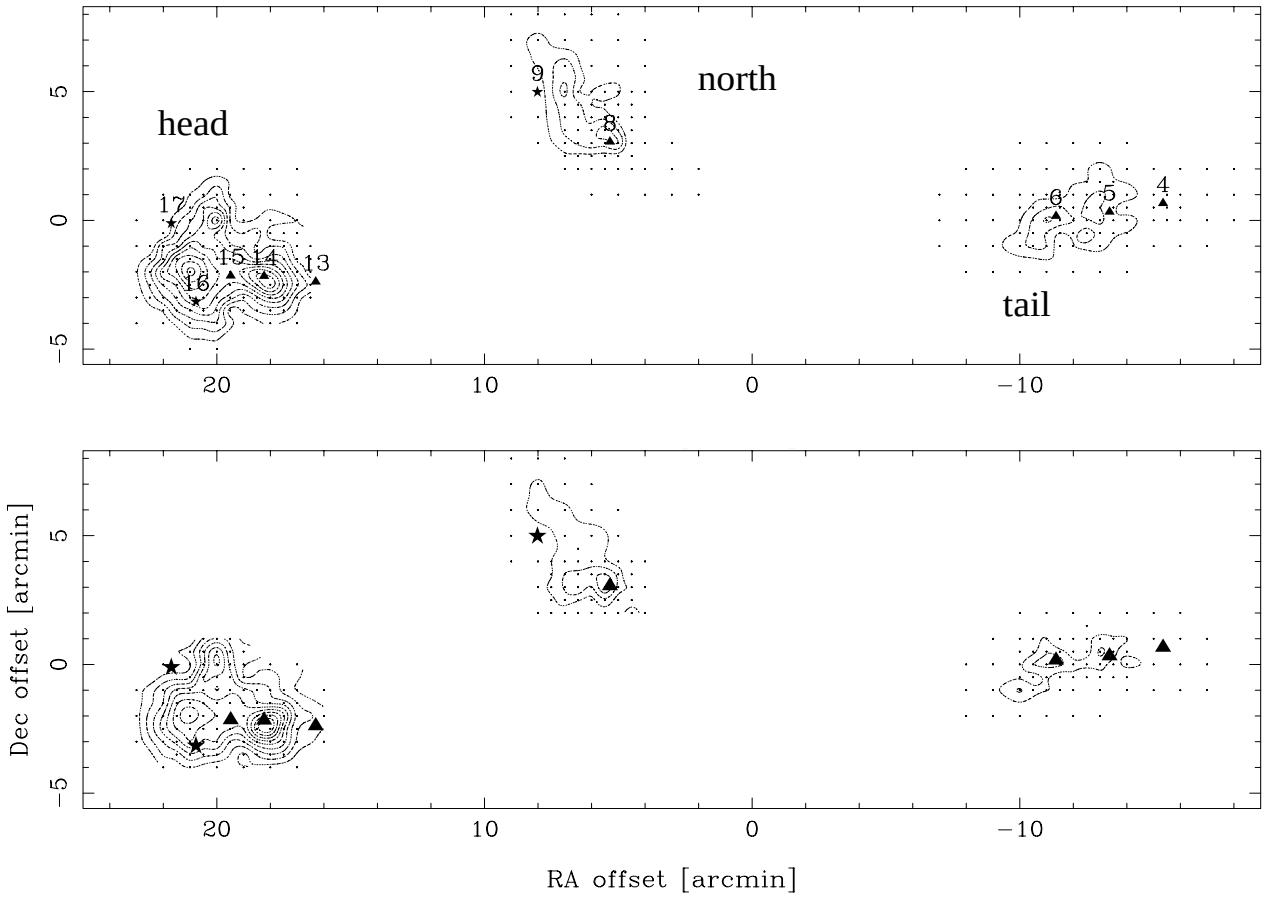

Fig. 2. HNC (upper panel) and HCN (lower panel) integrated intensity maps of L 1251 in the (–2, –6.5) km s^{-1} velocity range (for HCN the velocity range of the main 2–1 component). The center position is the same as in Fig. 1 and the observed positions are indicated by dots. The intensity scale is in $T_{\rm A}^{*}{\rm d}v$ [K km s^{-1}] and contours start from 0.9 and increase by 0.45 increments to 4.5 for HNC and from 0.8 with a 0.4 increment to 4.0 K km s^{-1} for HCN. The stars denote the FIR point sources classified as T Tau stars, and the triangles those classified as embedded YSOs (from Kun & Prusti 1993).

3.1. Identification of cores

The maps show local maxima which roughly correspond to the ammonia cores detected by TW. Because of the denser sampling and the higher spectral resolution available in the present study we see, however, more structure than discernible in the previous NH_3 maps. Using the spatial – velocity information available, we have identified altogether 15 cores in the mapped region, most of which can be seen in all four lines. Some of the NH_3 cores of TW divide in our maps into two components. Following the nomenclature of TW we label the five cores studied in detail as H1a, H2a, H2b, N1a and T1a, where "a" and "b" indicate a presence of a secondary peak or a separate velocity component not resolved in the previous NH_3 observations.

Table 1 lists the identified cores in order of decreasing RA offset (i.e., in head–to–tail direction). The columns are: (1) core identification number; (2) line center velocity; (3, 4) core center in the RA and Dec offsets with respect to the center of the map; (5) full width at half intensity of the integrated emission corrected for the beam size; (6) the full halfwidth of the global line profile of the core; (7) virial mass; (8) mass calculated from $C^{18}O$ and (9) association with YSOs or T Tau stars *and* core designation following TW. The core size, D, is estimated from the extent of the half power intensity contour deconvolved with the beam assuming Gaussian shapes for the beam as well as for the source. In most cases cores are elliptical, and we use the geometrical mean of the major and minor axes to define the size. Virial masses are derived using the formula $M_{\rm vir} = 150\, D\, \Delta v^2$ (see Johansson et al. 1998). For 5 cores independent mass estimates are derived from the $C^{18}O$ observations as $M = 1.456 \times 10^{-13}\, N_{\rm C^{18}O}\, (D_{\rm s}^2 + D_{\rm b}^2)$, where $D_{\rm s}$ and $D_{\rm b}$ are source diameter and beam size at the corresponding frequency, respectively (see Nikolić et al. 2001).

We have calculated standard deviation of the core diameters for all available molecules to be in the range ~0.1 to ~0.3 pc. The emission extents of observed molecules agree, in most cases, within $\pm 1\sigma$ of the arithmetical mean of a core.

The large differences between masses estimated from the virial theorem and the $C^{18}O$ data, obvious in three cores, may possibly be linked to the presence of young stellar objects; enhanced turbulence and/or ordered motions like, e.g., outflows could cause the discrepances.

From the $C^{18}O$ data, Sato et al. (1994) derived a total gas mass in the head region of 65 $M_\odot$. Adding up our estimates of core masses in the same region, we arrive at ~75 $M_\odot$ (using

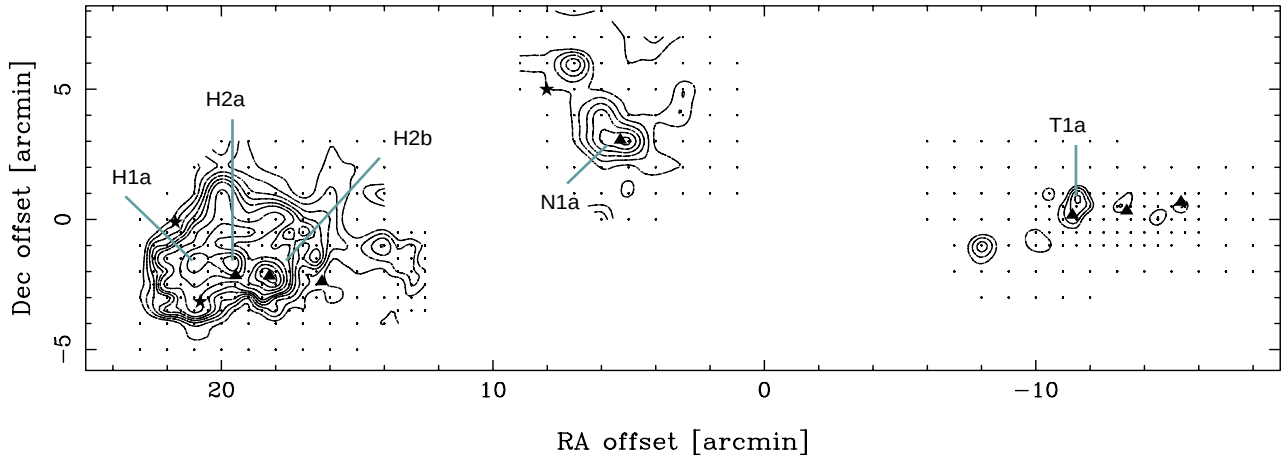

Fig. 3. The CS (2–1) integrated intensity map of L 1251. The velocity range of the emission, the center position, the intensity scale and markers are as in Fig. 1. Contours start from 0.65 to 1.3 by 0.13 K km s^{-1} and from 1.3 to 2.34 by 0.26 K km s^{-1}.

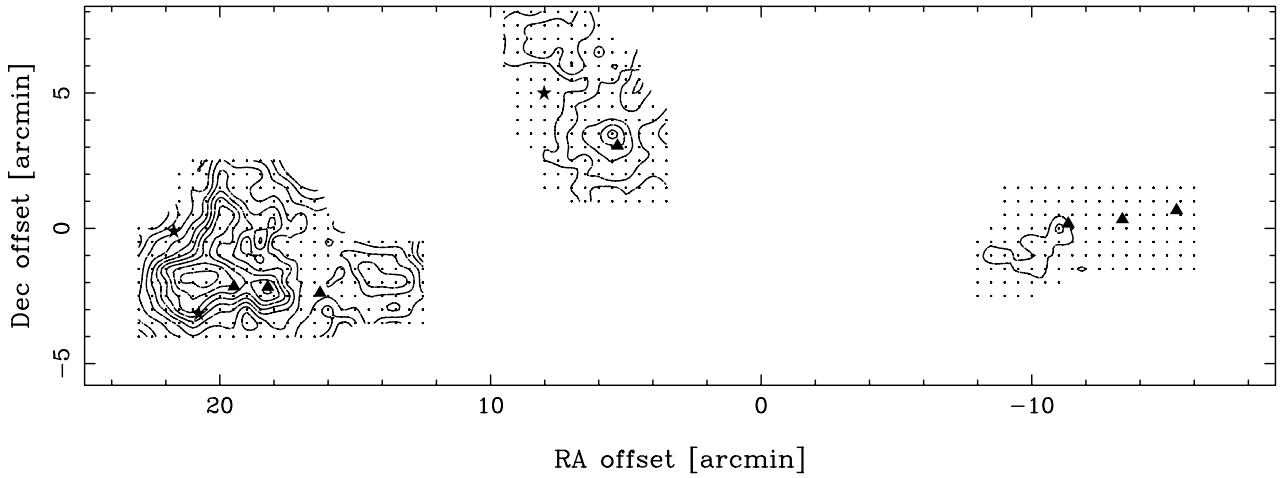

Fig. 4. The HCO^+ (1–0) integrated intensity emission map of L 1251 for the (–2, –8) km s^{-1} velocity range. The center position, the intensity scale and markers are as in Fig. 1. Contours start from 0.8 and increase by 0.45 K km s^{-1}.

M_{CO} where available, otherwise M_{vir}), indicating that most of the mass is concentrated in the dense cores. For the northern region of L 1251 Sato et al. (1994) estimate a total gas mass of 56 $M_\odot$. We derive a mass of 36 $M_\odot$ for core 7 (i.e. the N1a core) implying that for this region at least 65% of the total mass is in the form of dense gas.

3.2. Channel maps and decomposition of the "head" region

The observed emission in the head covers the range from –6 to –2 km s^{-1}, while the northern area and the tail are seen only in the ranges (–6, –4) and (–5, –3) km s^{-1}, respectively. This is consistent with the dominant velocity components of the ^{13}CO emission according to Sato et al. (1994).

Figure 3 shows the HNC (1–0) line emission of the head region in four velocity channels. The other observed lines show similar features in the corresponding channel maps. Two velocity components, centered at ≈–3.5 km s^{-1} and at ≈–4.5 km s^{-1} are clearly seen in the maps. These two velocity components are also discernible in the $HN^{13}C$ spectra of H1a, H2a and H2b.

3.3. An HCO^+ "disk" or a dense bipolar outflow?

Close inspection of the HCO^+ spectra in the N1a core area reveals a possible interaction with the CO outflow (Sato & Fukui 1989) within ∼2′ from the IRAS 22343+7501 source. At the estimated distance of the cloud this equals 36000 AU. In this area the line shapes of HCO^+ show significant wing emission between −8 and −2 km s^{-1} as well as self-absorption features. Figure 6 shows the extents of the blue– and red–shifted emission at the most extreme velocities. The structure presented mimics either a rotating HCO^+ "disk" or a "toroid" (see, e.g., Torrelles et al. 1983) around the protostar, or a dense HCO^+ outflow. The dashed line in Fig. 6 gives roughly the orientation of the CO outflow axes. If the structure is considered to be a disk, then the disk radius is ≈10 000 AU. Such large HCO^+ "disks" around low−mass protostars are not uncommon (see, e.g. Fridlund et al. 2002). On the other side, if we are observing a dense outflow, then the dynamical age is approximately the same for both wings and is equal to 2×10^4 years.

Table 1. Derived parameters from the CS (2–1) observations. Sizes and masses assume a distance of 300 pc.

Core	$v_{\rm lsr}$ [1]	$\Delta\alpha$	$\Delta\delta$	D	Δv	$M_{\rm vir}$ [2]	$M_{\rm CO}$ [3]	Comments [4]
	[km s^{-1}]	[′]	[′]	[pc]	[km s^{-1}]	[$M_\odot$]	[$M_\odot$]	
1	−4.8	21.0	−1.5	0.26	1.30	66	16	T Tau (H_α) #16; H1a
2	−4.2	20.0	−0.5	0.16	0.75	14		
3	−3.3	19.5	−1.5	0.14	0.74	11	11	T Tau candidate star #15; H2a
4	−4.3	18.5	−2.0	0.16	1.68	70	8	embedded YSO #14, compact outflow; H2b
5 [a]	−3.6	14.0	−1.5	0.13	1.15	26		H 3
6 [b]	−4.6	7.0	6.0	0.16	0.98	23		T Tau candidate star #9; N 2
7	−5.0	5.5	3.5	0.25	1.21	55	36	embedded YSO #8, extended outflow; N1 a
8 [c]	−4.4	−8.0	−1.0	0.13	0.66	8		
9	−4.4	−10.0	−1.0	0.13	0.76	11		
10 [d]	−4.1	−10.5	1.0	0.09	0.93	12		
11	−4.3	−11.5	0.0	0.15	0.97	18	4	embedded YSO #6; T1a
12 [d]	−4.2	−12.5	−0.5	0.07	0.75	6		
13 [b]	−4.0	−13.0	0.5	0.08	0.76	7		embedded YSO #5; T 2
14 [d]	−4.3	−14.5	0.0	0.09	1.12	14		
15 [d]	−4.4	−15.5	0.5	0.08	0.97	11		embedded YSO #4; T 3

[1] Gaussian fitted line center velocity at the peak position of the core.
[2] $M_{\rm vir} = 150\, D\, \Delta v^2$ (Johansson et al. 1998).
[3] $M_{\rm CO} = 1.456 \times 10^{-13}\, N_{\rm C^{18}O}\, (D_{\rm s}^2 + D_{\rm b}^2)$.
[4] IRAS point sources and detected outflows that fall within the half intensity contour of the core emission. The positions observed in the rarer isotopomers are also indicated.
[a] Surveyed only in CS and HCO^+. [b] Not detected in HCO^+. [c] Not detected in HCN. [d] Detected only in CS.

Table 2. Total column densities derived using the LTE assumption (see the text). For the three cores in the "head" appropriate velocity components were used (see Table 1). The formal errors are 10–15%, which include intensity calibration (∼10%) and spectral noise.

Molecule	[cm^{-2}]	H1a	H2a	H2b	N1a	T1a
^{13}CO	[10^{15}]	6.1	5.9	7.5	13.9	7.9
C^{18}O	[10^{15}]	1.2	1.9	1.6	2.7	1.1
C^{34}S	[10^{11}]	4.3	7.7	11.5	14.0	11.2
H^{13}CN	[10^{11}]	2.5	5.4	3.7	2.1	6.6
HN^{13}C	[10^{11}]	4.4	7.6	6.3	5.5	13.8
H^{13}CO$^+$	[10^{11}]	4.0	5.8	3.7	8.6	4.6
SO	[10^{13}]	1.8	1.0	1.0	0.7	1.0
NH_3 [a]	[10^{14}]	18	–	9.9	–	22

[a] From TW; velocity components of the cores in the head are not resolved.

4. Column densities and relative abundances

Table 2 gives column densities, derived assuming LTE conditions and optically thin emission, towards selected positions. In addition, it was assumed that the excitation temperature, $T_{\rm ex}$, is 10 K for ^{13}CO and C^{18}O, and 6 K for the other species which are likely to be subthermally excited (see, e.g., Caselli et al. 2002). The column densities of C^{34}S and HN^{13}C show the largest variations across the cloud. The C^{34}S column density has a minimum towards H1a in the head, whereas HN^{13}C peaks towards T1a in the tail. The column densities of the other molecules change less than by a factor of three. A comparison between different molecules brings forth some pairs with large variations in the column density ratios, and others with minor changes. For example, H^{13}CO$^+$/C^{18}O and HN^{13}C/H^{13}CN are roughly constant (∼3×10^{-4} and ∼2, respectively), C^{34}S/SO has by far the lowest value towards H1a, and HN^{13}C/C^{18}O is clearly largest towards T1a.

We have estimated also the H_2 column densities, $N(H_2)$, with the aid of C^{18}O and the conversion factor [C^{18}O]/[H_2] = 1.7×10^{-7} determined by Frerking et al. (1982). The $N(H_2)$ values have been then used to derive the fractional abundances of other observed molecules. In the conversion to the main

Table 3. H_2 total column densities (in [10^{21} cm^{-2}]) obtained from ^{13}CO using a conversion factor of $N(H_2)/N(^{13}CO) = 4.8 \times 10^5$ (Dickman & Clemens 1983) and from C^{18}O using the ratio [C^{18}O]/[H_2] = 1.7×10^{-7} (Frerking et al. 1982), and the calculated fractional abundances of the main isotopomers with respect to [H_2] derived from [C^{18}O].

		H1a	H2a	H2b	N1a	T1a
[^{13}CO] ⇒ [H_2]		2.93	2.84	3.58	6.67	3.77
[C^{18}O] ⇒ [H_2]		6.76	11.41	9.65	16.06	7.12
CS	[10^{-9}]	1.4	1.5	2.6	1.9	3.4
HCN	[10^{-9}]	2.9	3.6	2.9	1.0	7.1
HNC	[10^{-9}]	5.0	5.2	5.0	2.6	14.9
HCO^+	[10^{-9}]	4.6	3.9	3.0	4.1	4.9
SO	[10^{-9}]	2.8	0.7	1.0	0.5	1.3
NH_3	[10^{-7}]	2.6	–	1.0	–	3.1

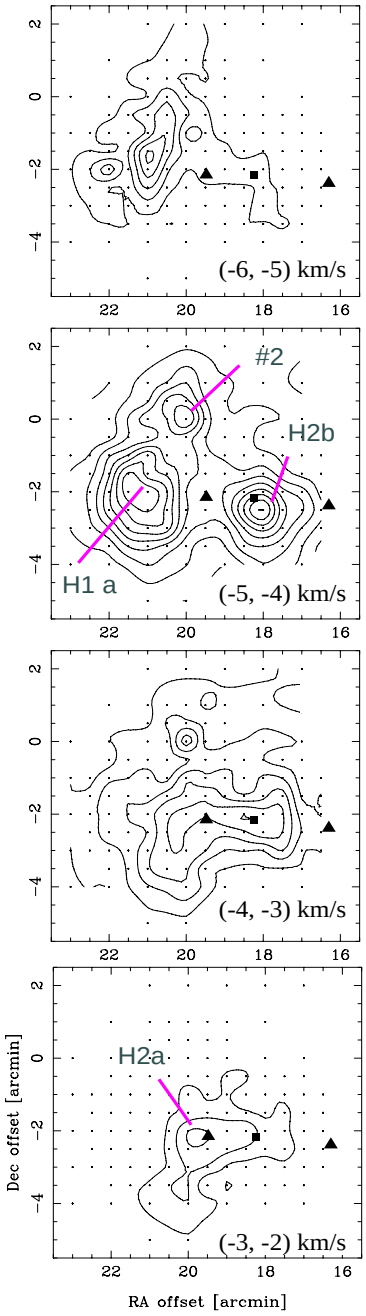

Fig. 5. The HNC channel velocity maps of the "head" region. The observed positions are indicated by dots. The intensity scale is in $T_A^* \mathrm{d}v$ [K km s^{-1}] and the contours start from 0.15 and are increasing by 0.3 K km s^{-1}. The velocity ranges are given in the lower right corners. Embedded YSOs are marked with triangles and the YSO suspected to be driving the compact outflow is marked by a rectangle. Additionally, our core designations are given in the second and fourth panel.

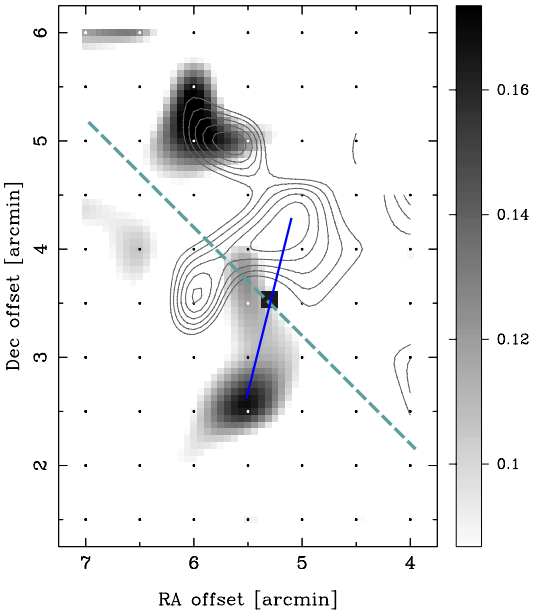

Fig. 6. Integrated intensity map of the blue – (greyscale) and the red–shifted (contours) HCO^+ emission of the N1a core. The velocity ranges are (–7, –8) and (–2, –3) km s^{-1} for the blue and the red wings, respectively. The intensity scale is in $T_A^* \mathrm{d}v$ [K km s^{-1}] with contours from 0.09 by an increment of 0.01 K km s^{-1}. The filled square marks the position of IRAS 22343+7501, the solid line marks the proposed disk and the dashed line shows the orientation of the corresponding CO outflow.

isotopomers fractional abundances the following isotopic ratios characteristic of the local ISM have been used: $^{12}C/^{13}C = 77$ and $^{32}S/^{34}S = 22$ (Wilson & Rood 1994). The H_2 column density estimates and the fractional abundances are given in Table 3. According to this table the position H1a has the lowest CS abundance and the largest SO abundance. The fractional HCN and HNC abundances seem to peak towards T1a. N1a, with the highest H_2 (in fact $C^{18}O$) column density, has the lowest SO abundance. In the other molecules the changes are less marked. It should be noted that the fractional abundances derived here reflect column densities relative to $C^{18}O$, and do not represent the true relative abundances with respect to H_2 in case the $C^{18}O/H_2$ column density ratio changes, e.g., due to CO depletion.

5. Estimates of temperatures from CH_3CCH

Symmetric top molecules, like methyl cyanide, CH_3CN, and methyl acetylene, CH_3CCH, make good temperature probes because each K–component of a given J rotational transition has a different energy level. Radiative transitions between different K–ladders are prohibited by the selection rule $\Delta K = 0$; thus the populations of different K-ladders are determined by collisions and depend mostly on the gas kinetic temperature. Also, being relatively close in frequencies, all K components can be observed simultaneously, avoiding calibration problems.

The $J = 5 - 4$, $K = 0, 1, 2, 3$, transitions of methyl acetylene were observed towards the previously selected five cores in L 1251. Figure 7 shows the spectra. To estimate kinetic temperatures we have used the rotational diagram method (see, e.g., Anderson et al. 1999) which assumes LTE conditions and optically thin emission. The derived rotational temperatures are unexpectedly high as are the associated errors. The reason for this can be traced back to the intensity of the $K = 0$ relative to the $K = 1$ transition; with the exception of the region H1a, the observed ratios all indicate $T_{\mathrm{rot}} > 50$ K. Such results can be explained in terms of non – LTE excitation or that the

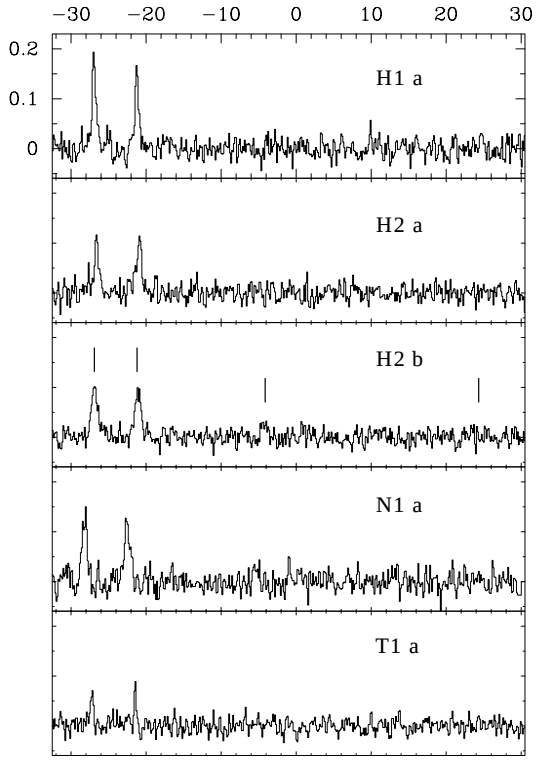

Fig. 7. The observed CH_3CCH 5–4 spectra smoothed to a velocity resolution of 0.12 km s^{-1}. Core designation is given in the upper right corner and the observed $K = 0, 1, 2, 3$ transitions are marked with solid lines. The intensity scale is T_A^* [K], and the velocity scale is v_{LSR} [km s^{-1}].

Table 4. The results of the CH_3CCH rotational diagram method weighted with observational errors plus E, A species uncertainties (case I) and using the $K = 1$ and $K = 2$ lines only (case II). Ammonia temperatures are from TW.

	H1a	H2a	H2b	N1a	T1a
case I					
T_{rot} [K]	27 ± 6	16 ± 5	18 ± 2	23 ± 2	22 ± 7
N_{tot} [10^{12} cm^{-2}]	31 ± 8	16 ± 8	21 ± 4	27 ± 5	8 ± 3
case II					
T_{rot} [K]	15 ± 4	8 ± 2	15 ± 2	16 ± 3	10 ± 5
N_{tot} [10^{12} cm^{-2}]	25 ± 2	27 ± 5	23 ± 1	28 ± 2	8 ± 1
$T_{21}^{NH_3}$ [K]	10	12	14	–	10

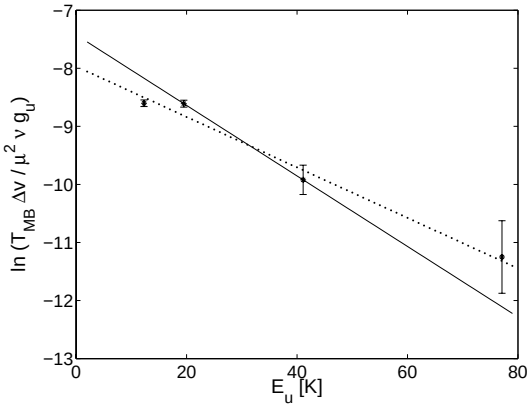

Fig. 8. Rotation diagram of the CH_3CCH 5–4 transition for core N1a. For definition of case I (dotted line) and case II (solid line) see the text and Table 4. The error bars refer to the observational uncertainties only.

total abundances of the A ($K = 0$) and E ($K = 1$) species are not equal. Assuming $T_{rot} = 15$ K, the E/A population ratio would be about 1.5 based on the $K = 0$ and 1 transitions. Askne et al. (1984) find that statistical equilibrium and rotational diagram calculations agree, with the exception of cold regions. Their analysis indicate that the total abundances of the A and E species are equal, however, defined by different partition functions at low kinetic temperatures. For TMC – 1, their observations show an intensity ratio of ∼1 between the $K = 0$ and 1, $J = 5$–4 transitions, while the statistical equilibrium analysis indicates $T_K \sim 10$ K and $T_{rot} \sim 6$ K. Observationally, this is very similar to our sample (with the exception of H1a), possibly indicating that this head core is warmer than the rest of the cores observed here.

To proceed we have introduced an uncertainty in the A and E species populations of 30%. The results are given as "case I" in Table 4 and clearly show smaller errors in the derived parameters in spite of larger total errors in the input data, a reflection of the inconsistent intensities of the $K = 0$ and 1 transitions. Figure 8 shows graphically this inconsistency common for all our cores with the exception of H1a. In "Case II" we have only used the $K = 1$ and 2 transitions (i.e. the E–species) to estimate the rotation temperatures. These results are further discussed in Sect. 6.4.

6. Discussion

6.1. Kinematics of the cloud

Our high spectral resolution observations have revealed two distinct velocity components in the head region, separated by about 1 km s^{-1}. The same components are most likely present in other molecules as well. The fact that these were interpreted as velocity gradients by TW is due to their cruder velocity resolution.

Similarly, a superposition of these two components at least partly explains the observed CS line asymmetry, i.e., "the infall profiles" seen by Mardones et al. (1997) towards IRAS 22376+7455. Yet a possible infall of dense gas cannot be ruled out.

6.2. YSOs and T Tau stars in dense cores

Five out of six embedded YSOs, as proposed by KP in the region we have surveyed, are most likely associated with the denser parts of L 1251: FIR sources #4, #5 and #6 in the tail area (associated with the cores 15, 13 and 11 in Table 1, respectively), source #8, (IRAS 22343+7501) in the northern area with core 7 (N1a) and source #14 (IRAS 22376+7455) with

core 4 (H2b). Additionally, based on their projection onto dense areas, three T Tau candidate stars are probably associated with the cloud: sources #16 and #17 in the topmost part of the head area and source #9 in the northern area of the cloud, all coincident with detected H α emission stars. Sources #13 and #15 in the head area are both blended by the strong IR emission from IRAS 22376+7455, and have ill–defined error ellipses. Since the former source does not seem to be associated with any dense core it may be either only projected on the cloud area or is a faint, low – mass embedded star (Kun, priv. com.). The position of source #15 correlates well with the center of core 3 (see Fig. 5), where the HCN peak integrated emission is $\sim$2.5 K km s^{-1}. Yun et al. (1999) derived an 80% likelihood of tracing an embedded Class 0 YSO if the detected HCN emission is stronger than 3 K km s^{-1}. Thus, source #15 may be an embedded Class 0/I YSO.

To derive the SFE of the cores we assume $M_* \sim 1\,M_\odot$ for all the embedded YSOs and T Tau stars with unknown masses, i.e., sources #6, #15, #16 and #17. IRAS 22376+7455 and IRAS 22343+7501 have estimated masses of 1.78 $M_\odot$ and 2.35 $M_\odot$, respectively (Kun 1998). If we use the masses of the cores listed in Table 1 ($M_{\rm CO}$), SFEs for the H1a, H2a, H2b, N1a and T1a cores are approximately 11%, 9%, 18%, 6% and 20%, respectively. On average, SFE of the observed cores would be $\sim$13%, almost 3 times lower than the previously estimated SFE for the whole cloud, but still 5–6 times higher than the overall SFE for the Galaxy.

6.3. Nature of IRAS 22343+7501

Based on IRAS and sub-mm continuum observations Mardones et al. (1997) derived the bolometric temperature of IRAS 22343+7501 to be $\leq$108 K, and classified the source as a Class I YSO. Using Chen et al. (1995) empirical relation between age and bolometric temperature for YSOs with $T_{\rm bol} \leq 1000$ K, we estimate IRAS 22343+7501 to be $(1.3 \pm 0.1) \times 10^4$ years old. This age would classify the source as a very young Class I YSO. Sato et al. (1994) derived the dynamical timescale (using an inclination of 45°) of the CO outflow to be 9.2×10^4 and 1.8×10^5 years for the blue– and the red–wing, respectively. Provided that IRAS 22343+7501 is the CO outflow driving source, consistent age estimates would require that the flow plane is close to the plane of sky, i.e., tilted by 4–8°. Kun (1998) estimated the mass of a hypothetical central star to be $M_* = 2.35\,M_\odot$. Near – infrared images (Rosvick & Davidge 1995) and recent 3.6 cm and 6 cm VLA continuum observations (Grissom Meehan et al. 1998; Beltrán et al. 2001) show that this IRAS source actually consists of several protostellar objects. The near – IR images exhibit a 20–30″ large nebulosity corresponding to a maximum size of 9000 AU. VLA continuum measurements revealed two sources, separated by 7″, i.e., about 2000 AU. Both continuum sources have spectral indices consistent with thermal emission, and any of them could be the CO outflow driving source (Beltrán et al. 2001). The proposed HCO^+ disk would encompass both sources.

Under the assumption that the properties of the HCO^+ emission (see Fig. 6) are similar to those in the N1a core, i.e., $I(HCO^+)/I(H^{13}CO^+) \approx 7$, we derive a total mass of this feature as $M = 50{\times}I_{MB}(HCO^+)\ A\ [M_\odot]$, where I_{MB} is the velocity integrated emission [K km s^{-1}] and A is the area of the HCO^+ wing emission [pc^2]. It is further assumed that the isotopic abundance ratio is 77 and that the fractional abundance of HCO^+ is 4×10^{-9} (see Table 3). The total wing emission integrated over the full velocity range and wings areas is 0.1 K km s^{-1}, yielding $\approx$5 $M_\odot$ of molecular gas, equally distributed between the approaching and receding emission regions.

Assuming that this emission originates from a disk rotating with a velocity of $\sim$2 km s^{-1} at its outer edge we find the centrifugal force to be $\sim$12 times larger than the gravitational force of the central star and the "disk" combined. Since the observed radial velocity is only a lower limit to the "rotation velocity", this factor (proportional to $v_{\rm rot}/M$) can most likely be considered as a lower limit, although our derived mass could be underestimated if the HCO^+ is more saturated than in the surroundings. However, the $H^{13}CO^+$ spectrum toward the IRAS source (N1a core center) shows no signs of wing emission, indicating a saturation level of the main isotope emission similar or lower than assumed. Based on our high ratio of centrifugal to gravitational forces we thus find it unlikely that the observed HCO^+ wing emission defines a disk.

On the other hand, if the observed structure represents a dense outflow, the derived dynamical age of the flow is 2×10^4 years (not corrected for an unknown inclination), i.e., an order of magnitude less than the CO outflow. The discrepancy between the dynamical ages for the CO and the suggested HCO^+ outflow indicates that they are of different origin. This is further emphasized by the apparently different orientations of the flows in the plane of the sky as well as in the radial direction (in contrast to CO, the red– and blue–emission regions of HCO^+ partly overlap). As noted earlier, we can probably treat the derived mass of $\sim$5 $M_\odot$ in the HCO^+ wings as an upper limit. We define a lower limit by assuming optically thin HCO^+ wing emission and arrive at $\sim$0.5 $M_\odot$. Using this range of masses, the released kinetic energy of the HCO^+ flow is estimated to be 4–40 $\times 10^{36}$ J and mechanical luminosity to be 1–10 $\times 10^{25}$ J/s i.e., 0.03–0.3 $L_\odot$; the lower limit comparable to the mechanical luminosity of the CO outflow although the CO outflow is spread over an area of the order of a magnitude larger. In this picture of two outflows traced by the CO and the HCO^+ emission, both continuum sources of Beltrán et al. (2001) could be protostars each driving its own outflow.

6.4. HCN/HNC ratios and kinetic temperatures

According to gas – phase chemical models the main route for production of HCN and HNC is by dissociative recombination with electrons (e.g. Hirota et al. 1998):

$$HCNH^+ + e^- \rightarrow HNC + H,\quad HCN + H. \qquad (1)$$

Based on their observations of starless and star forming cores, Hirota et al. (1998) derived a branching ratio of the reaction of 0.4 for the HNC production. The branching production ratio of HCN, α, is defined as [HCN]/[HNC] = $\alpha/1-\alpha$, if

$T_{\rm kin} \ll T_{\rm c}$, where $T_{\rm c} \approx 24$ K is the threshold temperature above which neutral–neutral reactions dominate the HCN/HNC ratio. We have estimated α in the directions of the sample cores. In the head part of L 1251 both *total* emission and the previously defined core emission is considered. All cores i.e., H1a, H2a, H2b, N1a and T1a have a branching production ratio of HCN in the range $\alpha = 0.2$–0.4. Similar values in the H2a/b cores are observed also when the total velocity ranges of the HCN and HNC emission are considered. However, towards the H1a core the branching ratio for the HCN production of the *total* emission is as high as $\alpha = 0.8 \pm 0.1$. The latter ratio is probably a reflection of more energetically favorable paths for destruction of HNC once the temperature of the gas exceeds the critical temperature in the region. Thus, this ratio indicates $T_{\rm kin} \geq 24$ K, while the rest of the cores are colder. This pattern is favored by the temperatures derived from our CH_3CCH observations (Table 4), although one should bear in mind the relatively large errors. However, as pointed out in Sect. 4 there are indications that the partition function of the *A* and *E* species deviate at low temperatures and, in our simple analysis, overestimate the temperatures. This effect would then apply to all our cores except towards H1a.

In conclusion, our HCN/HNC and CH_3CCH results favor a kinetic temperature in excess of ∼25 K towards H1a and less or significantly less than ∼20 K for the rest of the cores. This temperature increase of the dense gas is likely caused by shocks originating from outflows and/or radiation from the embedded stars. We searched the 2MASS All Sky Catalog and in the head region of L 1251, clustered around the two H_α stars and the two embedded YSOs (#14 and #15), we found 23 point sources. This suggests that the head region of L 1251 is much more productive than the northern core (8 point sources), and the tail cores (6 point sources). Regarding the possibility of external heating, the newly born pre–main sequence stars observed by KP could, in principle, heat the outer parts of the cloud to 20–25 K. However, there the gas density is too low to excite the molecular transitions observed by us. Another possibility, as suggested in the Introduction, is that the cloud has encountered at least one external shock; however such shocks have cooling times in a dense gas of the order of years (see, e.g., Smith & Rosen 2003).

6.5. Star formation and "Early-" and "Late–time" molecules

Based on the production pathways via ion-molecule or neutral-neutral reactions, and their dependence on neutral carbon (C I), some molecules are classified either as "early-time" (10^4–10^6 years after the onset of chemistry) or "late-time" species (maximum abundances reached at steady state, after about 10^6–10^8 years of chemical evolution; e.g. Herbst & Leung 1989). Of the molecules discussed here HCO^+, SO and NH_3 are usually considered as late-time molecules; HCO^+ because it is formed from CO, and the latter two because their formation mechanisms involve relatively slow neutral-neutral reactions. SO is furthermore destroyed primarily by C I which at later stages is locked up in CO (e.g. Nilsson et al. 2000). CS forms early, but its abundance remains roughly constant because of recycling via HCS^+ (Nejad & Wagenblast 1999). The situation of HCN and HNC is less clear in this picture. The precursor ion, $HCNH^+$, is produced mainly via a reaction between NH_3 and the C^+ ion, thus involving both a typical "late-time" molecule and an ion characteristic of young chemistry.

In the recent models of Rawlings et al. (2002) it is shown that in an "H-rich" environment the nitrogen chemistry is initiated at an early stage, and because of the less effective destruction of He^+ (due to a low CO abundance), NH_3 forms quickly thereafter. Under these circumstances also HNC is produced at early times via C + NH_2. NH_2 forms from a dissociative recombination of NH_3^+, which is one of the precursors of ammonia. In the "H-poor" models of Rawlings et al., on the other hand, the formation of HCN is efficient via N + CH_2 or N + CH_3 at early times. From these results one can expect that at early stages of chemical evolution the HCN/HNC abundance ratio depends strongly on the initial H content.

The division of molecules into "early–time" and "late–time" species is valid eventually only until a protostar is formed in a core, as this may change the physical conditions and consequently the chemical composition of the ambient cloud via heating of dust grains, enhanced turbulence and radiation field (see, e.g. Nejad et al. 1990). As a consequence of intensified desorption and ionization, we are then able to observe characteristically "young" chemistry.

X−ray surveys of star forming regions showed that Class I–III YSOs have significant X−ray emission (e.g., Getman et al. 2002; Casanova et al. 1995). The heating effect of this emission is very localized (e.g., Lepp & McCray 1983), but the X−ray induced ionization affects the whole core/cloud. Casanova et al. (1995) derived X−ray induced ionization rate throughout the ρ Oph cloud core to be comparable with the usually assumed cosmic rays ionization rate of $\sim 10^{-17}$ s^{-1}. A paradoxical situation may occur in the sense that a dynamically older core, with a central Class 0 embedded YSO is chemically younger than a pre-protostellar core (Kontinen et al. 2000).

All the dense cores studied here are associated with protostars or newly born stars: the presence of T Tau stars in the vicinity of H1a would indicate a dynamical age $\geq 10^6$–10^7 years for this core, while the embedded YSOs (#6, #8, #14 and #15) in the remaining 4 cores point to ages of 10^4–10^5 years, with the tail core being the youngest. The fact that H1a is located near the compression front corroborates the notion that the core is the most evolved among the L 1251 cores.

The fractional abundances given in Table 3 and the column density ratios given in Table 5 show some differences but lack clear trends with respect to the adopted dynamical ages of the cores. The large SO/CS and NH_3/CS column density ratios in H1a in the head conform with the idea that this core has reached an advanced stage of evolution. However, as discussed above one would possibly expect the presence of a T Tau star to alter the chemistry towards "younger" stages. This suggests that the influence of this T Tau star is hardly significant, provided that present chemical networks of dense and cold clouds predict the evolution of molecular abundances in a rather accurate way. On the other hand, the relatively low CO and HCO^+ column densities in T1a with respect to NH_3 and HNC (see Table 3) can

Table 5. Ratios of column densities, based on Table. 3. Relative errors of the ratios are in the range of 5–15%, for SO, CS, HCO^+ and HNC. For ratios that include ammonia, errors are in the range 20–25%.

	$\frac{[SO]}{[CS]}$	$\frac{[HCO^+]}{[CS]}$	$\frac{[NH_3]}{[CS]}$	$\frac{[SO]}{[HNC]}$	$\frac{[HCO^+]}{[HNC]}$	$\frac{[NH_3]}{[HNC]}$
H1a	2.0	3.2	186	0.6	0.9	53
H2a	0.5	2.6	–	0.1	0.8	–
H2b	0.4	1.1	39	0.2	0.6	20
N1a	0.2	2.1	–	0.2	1.6	–
T1a	0.4	1.4	90	0.1	0.3	20

be understood in two alternative ways: first, T1a can be in an early stage and CO and HCO^+ have not yet had time to reach the steady state abundances. This alternative would then imply that NH_3 and HNC are here early time species, and according to the models of Rawlings et al. (2002) would indicate an initially "H–rich" environment. The second alternative, and in fact the more likely, is that CO and HCO^+ are depleted in T1a. Previous observations have namely shown that NH_3 can remain in the gas–phase in the situation where CO is heavily depleted (e.g., Willacy et al. 1998; Tafalla et al. 2002). These studies concern mainly starless cores, but may be valid for cores with low–mass protostars which have not affected their surroundings yet. The high fractional HNC and HCN abundances in T1a suggest furthermore that also these molecules are more resistant against freezing–out than CO and HCO^+. This may be attributed to the replenishment of the $HNCH^+$ ion via the reaction between NH_3 and C^+. For the rest of the cores, Table 5 shows no definite trends which allow age sequencing. At the very best, our analysis indicates a possibility to discriminate cores with dynamical ages $\leq 10^5$ years from those older than 10^6 years. However, to fully establish such a conclusion, a considerably larger sample of cores is needed.

7. Summary

We have completed a survey of dense cores in L 1251 in several high gas density tracers: HCN, HNC, CS and HCO^+. On the larger scales, all observed molecules have similar distributions, including that of the previously published NH_3 data. Velocity components observed are consistent with the ^{13}CO data by Sato et al. (1994). The "head" part of the cloud consists of two gas components, whose central velocities differ by about 1 km s^{-1}. Altogether 15 dense cores can be identified in our maps.

Around IRAS 22343+7501, which is proposed to power the extended CO outflow, we have detected HCO^+ wing emission, the distribution of which is resembling either a rotating disk or a dense outflow. Stability considerations seem to exclude a disk interpretation. If an outflow, the derived dynamical age and apparent orientations suggest that its origin is most likely different from that of the CO outflow. In the direction of IRAS 22343+7501 Beltrán et al. (2001) have detected two continuum sources, separated by 7″, having spectral indices consistent with thermal emission. Thus, both sources could be protostars each driving its own outflow.

We have made additional observations towards five cores in SO, CH_3CCH and rare isotopomers of the mapped molecules in the selection. Using methyl acetylene and the HCN/HNC ratios as thermometers, we find a "temperature gradient" in the cloud. The highest temperature is detected in the head region.

The derived column density ratios do not change much from core to core. This is probably traceable to the fact that all cores are star forming and most of the molecules observed are characteristic of mature chemistry. Two of the cores have, however, peculiar abundance ratios. The core located in the tip of the "head" of the cloud, has clearly higher SO/CS and NH_3/CS ratios than seen anywhere else in the cloud, suggesting that the core has reached a very late stage of chemical evolution, probably assisted by an elevated temperature due to shock – heating in the head. In the other exceptional core, lying in the more quiescent "tail" of the cloud, the column densities of CO and HCO^+ are low compared with those of HNC, HCN, and NH_3. We suggest that this is due to depletion of CO and HCO^+, and as a corollary, that also HNC and HCN, like NH_3 belong to the molecules that remain longer in the gas phase than CO and HCO^+. The similar behavior of the former three molecules can probably be explained by their close relationship in the ion – molecule reaction schemes.

Four out of the five cores considered in L 1251 have embedded protostars in different stages of evolution. The revised average SFE of ∼10 % is almost 3 times lower than the previous estimate, but still ∼5 times higher than the overall SFE of the Galaxy. This high SFE indicates a contribution from externally triggered star formation.

Acknowledgements. The research was partly funded by the Ministry of Science and Technology of Serbia grant No. P1191 (2001-2004) and by the Finnish Center for International Mobility (CIMO). We are very grateful to Dr. M. Kun for the suggestion to use the 2MASS ASC, and to Dr. N. Mizuno who provided the ^{13}CO data presented in Fig. 1.

Onsala Space Observatory is the Swedish National Facility for Radio Astronomy and is operated by Chalmers University of Technology, Göteborg, Sweden, with financial support from the Swedish Natural Science Research Council and the Swedish Board for Technical Development.

References

Anderson, I. M., Caselli, P., Haikala, L. K., & Harju, J. 1999, A&A, 347, 983

Askne, J., Höglund, B., Hjalmarson, Å., & Irvine, W. M. 1984, A&A, 130, 311

Balázs, L. G., Eisloeffel, J., Holl, A., Kelemen, J., & Kun, M. 1992, A&A, 255 281

Beltrán, M. T., Estalella, R., Anglada, G., Rodríguez, L. F., & Torrelles, J. M. 2001, AJ, 121, 1556

Berkhuijsen, E. M. 1971, A&A, 14, 252

Casanova, S., Montmerle, T., Feigelson, E. D., & André, P. 1995, ApJ, 439, 752

Caselli, P., Benson, P. J., Myers, P. C., & Tafalla, M. 2002, ApJ, 572, 238

Claussen, M. J., Wilking, B. A., Benson, P. J., et al. 1996, ApJS, 106, 111

Dickman, R. L., & Clemens, D. P. 1983, ApJ, 271, 143

Eiroa, C., Torrelles, J. M., Miranda, L. F., Anglada, G., & Estalella, R. 1994, A&AS 108, 73

Frerking, M. A., Langer, W. D., & Wilson, R. W. 1982, ApJ, 262, 590
Fridlund, C. V. M., Bergman, P., White, G. J., Pilbratt, G. L., & Tauber, J. A. 2002, A&A, 382, 573
Getman, K. V., Fiegelson, E. D., Townsley, L., et al. 2002, ApJ, 575, 354
Grenier, I. A., Lebrun, F., Arnaud, M., et al. 1989, ApJ, 347, 231
Grissom Meehan, L. S., Wilking, B. A., Claussen, M. J., Mundy, L. G., & Wootten, A. 1998, AJ, 115, 1599
Herbst, E., & Leung, C. M. 1989, ApJS, 69, 271
Hirota, T., Yamamoto, S., Mikami, H., & Ohisi, M. 1998, ApJ, 503, 717
Johansson, L. E. B., Greve, A., Booth, R. S., et al. 1998, A&A, 331, 857
Kontinen, S., Harju, J., Heikkilä, A., & Haikala, L. K. 2000, A&A, 361, 704
Kun, M. 1982, Afz, 18, 63
Kun, M. 1998, ApJS, 115, 59
Kun, M., & Prusti, T. 1993, A&A, 272, 235
Kun, M., Vinkó, J., & Szabados, L. 2000, MNRAS, 319, 777
Lepp, S., & McCray, R. 1983, ApJ, 269, 560
Lynds, B. T. 1962, ApJS, 7, 1
Mardones, D., Myers, P. C., Tafalla, M., et al. 1997, ApJ, 489, 719
Myers, P. C., Dame, T. M., Thaddeus, P., et al. 1986, ApJ, 301, 398
Nejad, L. A. M., Williams, D. A., & Charnley, S. B. 1990, MNRAS, 246, 183
Nejad, L. A. M., & Wagenblast, R. 1999, A&A, 350, 204
Nikolić S., Kiss Cs., Johansson, L. E. B., Wouterloot J. G A., & Tóth L. V. 2001, A&A, 367, 694
Nilsson, A., Hjalmarson, Å., Bergamn, P., & Millar, T. 2000, A&A 358, 257
Rawlings, J. M. C., Hartquist, T. W., Williams, D. A., & Falle, A. E. G. 2002, A&A, 391, 681
Rosvick, J. M., & Davidge, T. J. 1995, PASP, 107, 49
Sato, F., Mizuno, A., Nagahama, T., et al. 1994, ApJ, 435, 279
Sato, F., & Fukui, Y. 1989, ApJ, 343, 773
Schwartz, P. R., Gee G., & Huang, Y.-L. 1988, ApJ, 327, 350
Smith, M. D., & Rosen, A. 2003, MNRAS, 339, 133
Tafalla, M., Myers, P. C., Caselli, P., Walmsley, C. M., & Comito, C. 2002, ApJ, 569, 815
Torrelles, J. M., Rodríguez, L. F., Cantó, J., et al. 1983, ApJ, 274, 214
Tóth, L. V., & Walmsley, C. M. 1994, IBVS, 4107
Tóth, L. V., & Walmsley, C. M. 1996, A&A, 311, 981
Tóth, L. V., & Kun, M. 1997, IBVS, 4492
Wilking, B. A., Claussen, M. J., Benson, P. J., et al. 1994, ApJ, 431, L119
Willacy, K., Langer, W. D., & Velusamy, T. 1998, ApJ, 507, 171
Wilson, T. L., & Rood, R. 1994, ARA&A, 32, 191
Xiang, D., & Turner, B. T. 1995, ApJS, 99, 121
Yun, J. L., Moreira, M. C., Afonso, J. M., & Clemens, D. P. 1999, AJ, 118, 990